Research Article

Mathematical Methods in the Applied Sciences

Received 12 July 2013

Published online 11 March 2014 in Wiley Online Library

(wileyonlinelibrary.com) DOI: 10.1002/mma.3034
MOS subject classification: 76W99

Numerical simulations of thermal convection under the influence of an inclined magnetic field by using solenoidal bases

D. Yarımpabuç[a*†], H. I. Tarman[b] and C. Yıldırım[c]

Communicated by C. Miao

The effect of an inclined homogeneous magnetic field on thermal convection between rigid plates heated from below under the influence of gravity is numerically simulated in a computational domain with periodic horizontal extent. The numerical technique is based on solenoidal (divergence-free) basis functions satisfying the boundary conditions for both the velocity and the induced magnetic field. Thus, the divergence-free conditions for both velocity and magnetic field are satisfied exactly. The expansion bases for the thermal field are also constructed to satisfy the boundary conditions. The governing partial differential equations are reduced to a system of ordinary differential equations under Galerkin projection and subsequently integrated in time numerically. The projection is performed by using a dual solenoidal bases set such that the pressure term is eliminated in the process. The quasi-steady relationship between the velocity and the induced magnetic field corresponding to the liquid metals or melts is used to generate the solenoidal bases for the magnetic field from those for the velocity field. The technique is validated in the linear case for both oblique and vertical case by reproducing the marginal stability curves for varying Chandrasekhar number. Some numerical simulations are performed for either case in the nonlinear regime for Prandtl numbers $Pr = 0.05$ and $Pr = 0.1$.

Keywords: thermal convection; magnetic fields; solenoidal bases; legendre polynomials

1. Introduction

Magnetic field interacts with electrically conducting moving fluid through Lorentz force. Various experimental and numerical studies are performed to explore the consequences of this interaction between convective motions and magnetic field in the fields of metallurgy [1], astrophysics [2], flow control [3], and hydrodynamic stability [4]. It is observed experimentally [5] and verified theoretically [2] that when applied in the vertical direction (direction of gravity), an external magnetic field suppresses the roll motion arising in thermal convection between plates heated from below and thus delays the onset of convective motions. When applied in the horizontal direction, it aligns the convection rolls and stabilize the onset of oscillatory instability. The convective layer between plates of infinite extent provides the simplicity in geometry to focus on the interaction between thermal convection and the externally applied magnetic field. On a periodic geometry as convective cells, there have been series of numerical studies exploring the nonlinear interaction of a magnetic field and convection [6–11].

The equations modeling the interaction between buoyancy force and the Lorentz force are obtained from Navier–Stokes equations using Boussinesq approximation and Maxwell equations. In Boussinesq approximation, the density is treated as a constant in all terms except in the buoyancy term where variability with temperature is assumed. Thus, the convective flow field is still considered solenoidal (divergence-free). The numerical treatment of the solenoidal condition has been one of the most challenging aspects of computational incompressible fluid dynamics. Various treatment techniques have been employed in literature such as the fractional step [12], the influence matrix [13], and the staggered grid [14]) methods. The common focus in these techniques is to numerically treat the pressure variable, which usually comes without any boundary conditions and whose role is to enforce the solenoidal condition on the flow. On the other hand, these techniques help to enforce the solenoidal condition only to a certain limited degree of

[a] *Department of Mathematics, Osmaniye Korkut Ata University, Osmaniye, Turkey*
[b] *Department of Engineering Sciences, Middle East Technical University, Ankara, Turkey*
[c] *Department of Mechanical Engineering, Akdeniz University, Antalya, Turkey*
**Correspondence to: Durmuş Yarımpabuç, Department of Mathematics, Osmaniye Korkut Ata University, Osmaniye, Turkey.*
[†] *E-mail: durmusyarimpabuc@osmaniye.edu.tr*

accuracy. Accurate handling of the solenoidal condition is important in numerical hydrodynamic stability studies where the flow is perturbed to identify the critical parameter values between the transitory regimes. Furthermore, the numerical simulation studies of flow under the influence of a magnetic field encounter an additional solenoidal condition on the magnetic field variable. Various numerical approaches [7], [15] have been used for this purpose, and the effects of the poor handling of the solenoidal condition [16] and some remedies [17] are presented in literature.

In this work, solenoidal bases expansion is used in the numerical simulation of Rayleigh–Bénard thermal convection under the influence of an oblique magnetic field. By introducing an expansion in terms of solenoidal basis functions for the velocity and the magnetic field into the model equations in a Galerkin projection onto dual solenoidal bases, both solenoidal conditions are exactly satisfied and the pressure variable is completely eliminated, thus the number of equations and the number of flow variables are reduced. This reduces the burden on the numerical technique and increases the accuracy with which the solenoidal conditions are satisfied. While the velocity solenoidal basis functions are generated independently, a quasi-steady relationship between the velocity and the magnetic field variables is used to generate the corresponding magnetic solenoidal basis functions. This relationship arises in the case of liquid metals or melts as the convective fluid. The basis functions are expressed in terms of Legendre polynomials where they facilitate the construction of the dual bases and the evaluation of the Galerkin projection integrals using highly accurate Gauss–Legendre–Lobatto (GLL) quadrature rule.

Some early studies on the use of solenoidal bases are conducted by Leonard and Wray [18], Moser *et al*. [19], and Mhuiris [20] where shifted-Jacobi, Chebyshev, and Legendre polynomials are used for the representation of the solenoidal bases, respectively. They are the polynomial solutions to singular Sturm Liouville problems with weighted orthogonality property and exhibit excellent convergence properties. However, the need for the inclusion of the associated weight function in the construction of the dual bases makes Legendre polynomials the most convenient because of the associated unity weight. Other works employ solenoidal expansions in the form of generalized streamfunctions [21] or toroidal–poloidal decomposition [7, 9, 11] of a solenoidal vector field in order to exactly satisfy the continuity equation. Further, the procedure employed for eliminating the pressure leads to increased order of derivatives in the resulting evolution equations. More recently, Meseguer and Trefethen [22] presented a Galerkin procedure for the pipe flow using solenoidal basis functions based on Chebyshev polynomial representation. Techniques of spectral methods are employed in [22] leading to efficient implementation; however, the incorporation of the associated weight leads to added effort in the construction of the dual solenoidal bases. An analysis on the use of solenoidal bases in the numerical approximation of the Stokes problem is presented in [23]) and a domain decomposition procedure is proposed in [24] to introduce some flexibility in the use of solenoidal bases. Other solenoidal bases are constructed empirically from flow database and used for optimal truncated representation of the underlying flow field such as Karhunen–Loeve bases [25]. They are efficient in energy optimal low dimensional representation of the dynamics, but they are parameter dependent and carry the limited degree of accuracy in satisfying the solenoidal condition as the flow database.

The geometry of the problem, the system of model partial differential equations, dimensionless numbers, and the boundary conditions are presented in Section 2. In Section 3, solenoidal basis functions for the velocity and the magnetic field, which satisfy divergence-free and boundary conditions, are constructed, and the dual bases for velocity field are built on the basis of the condition of eliminating the total pressure term from the model system. In Section 4, a weak solution is obtained by applying Galerkin projection to the model partial differential equations. Then, the linear stability of the system is investigated by dropping the nonlinear terms involving perturbation variables over the basic conductive state, and the results are compared with the works of Chandrasekhar [2], Busse and Clever [10], and Burr and Müller [26]. The time discretization of the system and treatment of the nonlinear terms are explained for the simulations in the nonlinear regime in Section 5 where verification of the results are also presented. The results of the present work are compared with Güray and Tarman [27] and Busse and Clever [9].

2. Governing equations

Thermal convective motion of a perfectly conducting fluid is considered in a periodic horizontal layer of thickness d between conducting plates that are heated from below under the influence of a uniform magnetic field B_0 applied externally in the yz plane with angle χ from y axis (Figure 1).

The dimensionless form of the model equations are as follows:

$$\nabla \cdot \mathbf{u} = 0, \tag{1}$$

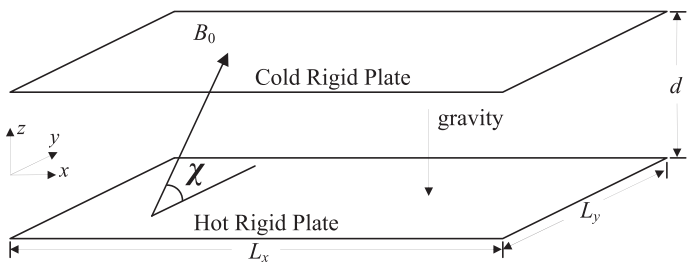

Figure 1. The geometry of the periodic convective domain.

$$\frac{\partial \mathbf{u}}{\partial t} = -(\mathbf{u}\cdot\nabla)\,\mathbf{u} - \nabla\Pi + PrRa_h\Theta\mathbf{e}_z + Pr\nabla^2\mathbf{u} + Q_hPr\left(Cos\chi\frac{\partial}{\partial y} + Sin\chi\frac{\partial}{\partial z}\right)\mathbf{b}, \tag{2}$$

$$\frac{\partial \Theta}{\partial t} + (\mathbf{u}\cdot\nabla)\,\Theta = \frac{w}{2} + \nabla^2\Theta, \tag{3}$$

$$\nabla^2\mathbf{b} = -\left(Cos\chi\frac{\partial}{\partial y} + Sin\chi\frac{\partial}{\partial z}\right)\mathbf{u}, \tag{4}$$

$$\nabla\cdot\mathbf{b} = 0, \tag{5}$$

where p denotes the pressure, $\mathbf{u} = (u, v, w)$ the velocity vector, $\mathbf{b} = (b_x, b_y, b_z)$ the induced magnetic field, and Θ is the deviation from the linear conductive temperature profile. The nondimensionalization is performed in accordance with Chandrasekhar [2], namely, thermal diffusion time is used as the time scale, temperature difference between plates ΔT as the temperature scale, and B_0 as the magnetic scale, except for the length scale, which is taken on the basis of the half depth $d_h = \frac{1}{2}d$ for computational convenience. The resulting dimensionless numbers are the Rayleigh ($Ra = 8Ra_h$), Chandrasekhar ($Q = 4Q_h$), and Prandtl (Pr) numbers where

$$Ra = \frac{g\,\triangle\, Td^3\alpha}{\kappa\nu},\quad Q = \frac{B_0^2d^2}{\rho\mu\nu\lambda},\quad Pr = \frac{\nu}{\kappa}. \tag{6}$$

Here, the Rayleigh and Chandrasekhar numbers, respectively, characterize the buoyancy and the Lorentz forces in relation to the viscous forces. Prandtl number is the ratio of the rates of the advection of momentum and heat and plays a role in the nonlinear regimes of convection. The appearance of Ra_h and Q_h in (2) is due to the use of half depth as the length scale.

Total magnetic field in the dimensionless form becomes

$$\mathbf{B} = Cos\chi\mathbf{e}_y + Sin\chi\mathbf{e}_z + \frac{\kappa}{\lambda}\mathbf{b}, \tag{7}$$

which indicates that the induced magnetic field $\mathbf{b}$ is weak compared with the externally imposed uniform magnetic field B_0 in a conducting fluid having the limit $\kappa \ll \lambda$ with κ and λ being thermal and magnetic diffusivities, respectively. In this limit, all the terms multiplied by $\frac{\kappa}{\lambda}$ is neglected in the induction equation

$$\frac{\kappa}{\lambda}\left(\frac{\partial \mathbf{b}}{\partial t} + \mathbf{u}\cdot\nabla\mathbf{b} - \mathbf{b}\cdot\nabla\mathbf{u}\right) = \left[\left(Cos\chi\mathbf{e}_y + Sin\chi\mathbf{e}_z\right)\cdot\nabla\right]\mathbf{u} + \nabla^2\mathbf{b}, \tag{8}$$

resulting in (4) and in Lorentz force

$$(\nabla\times\mathbf{B})\times\mathbf{B} = -\frac{1}{2}\nabla^2\mathbf{B} + \left[\left(Cos\chi\mathbf{e}_y + Sin\chi\mathbf{e}_z\right)\cdot\nabla\right]\mathbf{u} + \frac{\kappa}{\lambda}(\mathbf{b}\cdot\nabla)\,\mathbf{b}, \tag{9}$$

resulting in the corresponding term in (2) after the term $\nabla^2\mathbf{B}$ is combined in the gradient term $\nabla\Pi$, which is eliminated in the projection procedure. Liquid metals or melts are characterized by this limit.

The flow takes place in a doubly periodic three-dimensional rectangular region Ω in Figure 1 with aspect ratio $s_x \times s_y \times 2$ or $\Gamma\left[\frac{1}{2}s_x : \frac{1}{2}s_y\right]$ such that

$$0 \le x \le s_x,\quad 0 \le y \le s_y,\quad -1 \le z \le 1, \tag{10}$$

where $s_x = L_x/d_h$ and $s_y = L_y/d_h$ are the dimensionless periods in the horizontal x and y directions, respectively. While periodic boundary conditions are used for all the dependent variables in the horizontal directions, the boundary conditions at the perfectly conducting plates in the vertical that are maintained at constant temperatures take the form

$$\mathbf{u} = 0 \text{ and } \frac{\partial b_x}{\partial z} = \frac{\partial b_y}{\partial z} = b_z = \Theta = 0 \text{ at } z = \pm 1. \tag{11}$$

3. Solenoidal bases

At the outset, the solenoidal basis functions $\mathbf{V}(\mathbf{x})$ are required to satisfy

$$\nabla\cdot\mathbf{V} = 0,\quad \mathbf{V}(\mathbf{x})\,|_{z=\pm1} = \mathbf{0}. \tag{12}$$

The assumption of periodicity in the horizontal directions allows the use of Fourier representation

$$\mathbf{V}(\mathbf{x}) = \mathbf{V}(z)e^{(i\xi x + i\eta y)}, \tag{13}$$

and reduces the continuity equation to the form

$$i\xi U + i\eta V + \mathbb{D}W = 0, \tag{14}$$

where $\mathbf{V}(z) = (U, V, W)$ and $\mathbb{D} = \frac{d}{dz}$ are the differentiation operator. The same letter is used for both basis $\mathbf{V}(\mathbf{x})$ and its vertical profile $\mathbf{V}(z)$ here, and in the subsequent paragraphs for economy of notation, however, explicit appearance of the argument $\mathbf{x}$ or z is used to provide distinction where necessary. It turns out that the basis functions come in pairs $\mathbf{V}^{(j)}, j = 1, 2$ because the continuity equation reduces the degree of freedom in selecting the components of $\mathbf{V}$ to two by connecting the three components together. A typical set of solenoidal basis functions for the wavenumbers $\xi \neq 0$ and $\eta \neq 0$ are as follows:

$$\mathbf{V}_p^{(1)}(z) = \begin{bmatrix} -\eta g \\ \xi g \\ 0 \end{bmatrix}, \quad \mathbf{V}_p^{(2)}(z) = \begin{bmatrix} i\xi \mathbb{D}h \\ i\eta \mathbb{D}h \\ \gamma^2 h \end{bmatrix}, \tag{15}$$

and for $\xi = 0$ and $\eta = 0$

$$\mathbf{V}_p^{(1)}(z) = \begin{bmatrix} g \\ 0 \\ 0 \end{bmatrix}, \quad \mathbf{V}_p^{(2)}(z) = \begin{bmatrix} 0 \\ h \\ 0 \end{bmatrix}. \tag{16}$$

Here, $\gamma^2 = \xi^2 + \eta^2$, $g = (1 - z^2)L_p(z)$, $h = (1 - z^2)^2 L_p(z)$, and $L_p(z)$ denotes Legendre polynomial of degree p. The solenoidal basis pairs carry different characters in that while $\mathbf{V}^{(1)}$ lacks vertical velocity component $\mathbf{V}^{(1)} \cdot \mathbf{e}_z = 0$, $\mathbf{V}_p^{(2)}$ has vanishing vertical vorticity component $\left(\nabla \times \mathbf{V}_p^{(2)}\right) \cdot \mathbf{e}_z = 0$. In fact, the pairing of the bases corresponds to toroidal–poloidal decomposition of the flow field

$$\mathbf{u} = \nabla \times \mathbf{e}_z \psi + \nabla \times (\nabla \times \mathbf{e}_z \varphi), \tag{17}$$

for some functions ψ, φ [11].

For the subsequent projection procedure, dual basis functions $\overline{\mathbf{V}}^{(j)}(\mathbf{x})$ need to be constructed to satisfy

$$\nabla \cdot \overline{\mathbf{V}}^{(j)} = 0, \quad \overline{\mathbf{V}}^{(j)} \cdot \mathbf{e}_z \,|_{z=\pm 1} = 0. \tag{18}$$

These requirements on the dual bases facilitate the elimination of the gradient term $\nabla \Pi$:

$$\langle \overline{\mathbf{V}}, \nabla \Pi \rangle = \int_\Omega \overline{\mathbf{V}} \cdot \nabla \Pi \, d\Omega = \int_S \Pi \left(\overline{\mathbf{V}} \cdot \mathbf{n}\right) dS - \int_\Omega \Pi \left(\nabla \cdot \overline{\mathbf{V}}\right) d\Omega, \tag{19}$$

in the projection procedure under the inner product

$$\langle \mathbf{F}, \mathbf{G} \rangle = \int_\Omega \mathbf{F}(\mathbf{x}) \cdot \mathbf{G}(\mathbf{x}) \, d\Omega. \tag{20}$$

Here, $\mathbf{n}$ is the outward unit normal to the bounding surface S of the horizontally periodic convective domain Ω including the upper and lower plates where $\mathbf{n} = \pm \mathbf{e}_z$. A typical set of dual basis $\overline{\mathbf{V}}_p$ satisfying the study of Leonard and Wray (18) has the form as in (15) and (16) with the choices of $g = L_p(z)$, $h = (1 - z^2)L_p(z)$. Normally, a weight function $\omega(z)$ associated with the underlying expansion in the z variable appears in the inner product integral that causes the dual bases to satisfy the condition $\nabla \cdot \left(\omega(z)\overline{\mathbf{V}}\right)$ for the elimination of the gradient term. The use of underlying Legendre expansion associated with the unity weighting $\omega(z) = 1$ becomes advantages here in the construction for the dual bases in comparison with, for example, Chebyshev expansion associated with $\omega(z) = (1 - z^2)^{1/2}$.

Because the induced magnetic field $\mathbf{b}$ is prescribed by the velocity field as stated by the quasi-steady relationship (4), solenoidal basis functions

$$\mathbf{B}(\mathbf{x}) = \mathbf{B}(z) e^{(i\xi x + i\eta y)}, \tag{21}$$

for the magnetic field are constructed by solving

$$\mathbb{D}^2 \mathbf{B} - \gamma^2 \mathbf{B} = -\left[Cos\chi \eta_m i + Sin\chi \mathbb{D}\right] \mathbf{V}, \tag{22}$$

for $\mathbf{B}(z)$ subject to the boundary conditions

$$\mathbb{D}B_x = \mathbb{D}B_y = B_z = 0 \ \ at \ \ z = \pm 1. \tag{23}$$

for each $\mathbf{V} = \mathbf{V}_p^{(j)}(z)$, where $\mathbf{B}(z) = (B_x, B_y, B_z)$. The singularity in the equations for B_x and B_y at $\xi = \eta = 0$ due to the homogeneous Neumann boundary conditions is removed by setting

$$B_x(0) = B_y(0) = 0, \tag{24}$$

without loss of generality.

4. Numerical experiments

The assumption of periodicity in the horizontal directions allows the use of Fourier series expansions of the dependent flow variables,

$$\begin{bmatrix} \mathbf{u} \\ \Theta \\ \mathbf{b} \end{bmatrix}(x,y,z,t) = \sum_{m,n} \begin{bmatrix} \hat{\mathbf{u}} \\ \hat{\Theta} \\ \hat{\mathbf{b}} \end{bmatrix}(m,n,z,t) e^{(i\xi_m x + i\eta_n y)}, \tag{25}$$

where $\xi_m = \frac{2\pi m}{s_x}$ and $\eta_n = \frac{2\pi n}{s_y}$ are the wave numbers with the ranges $-\frac{1}{2}N_x + 1 \le m \le \frac{1}{2}N_x$ and $-\frac{1}{2}N_y + 1 \le n \le \frac{1}{2}N_y$ for the indices m and n. The vertical profiles for the velocity and the induced magnetic fields are further expanded in terms of the solenoidal bases

$$\hat{\mathbf{u}}(m,n,z,t) = \sum_{p=0}^{M} a_p^{(1)}(t)\mathbf{V}_p^{(1)}(z) + a_p^{(2)}(t)\mathbf{V}_p^{(2)}(z), \tag{26}$$

$$\hat{\mathbf{b}}(m,n,z,t) = \sum_{p=0}^{M} a_p^{(1)}(t)\mathbf{B}_p^{(1)}(z) + a_p^{(2)}(t)\mathbf{B}_p^{(2)}(z). \tag{27}$$

The velocity and the induced magnetic fields share the same time evolution as dictated by the quasi-steady link stated in (4). The expansion for the thermal field is taken as

$$\hat{\Theta}(m,n,z,t) = \sum_{p=0}^{M} b_p(t) T_p(z), \tag{28}$$

where $T_p(z) = (1-z^2)L_p(z)$ with its dual $\overline{T}_p(z) = L_p(z)$. The evolution of the time-dependent expansion coefficients $a_p^{(j)}(t)$ and $b_p(t)$ is determined by numerically integrating the projected model equations in time. For the numerical evaluation of the inner product integrals arising in the projection procedure, GLL quadrature is used

$$< \mathbf{f}, \mathbf{g} > = \int_{-1}^{1} \mathbf{f}^*(z) \cdot \mathbf{g}(z)\, dz \approx \sum_{q=0}^{N_z} w_q \mathbf{f}^*(z_q) \cdot \mathbf{g}(z_q), \tag{29}$$

where (w_q, z_q) are GLL quadrature weights and nodes, respectively. It can be shown that the number of quadrature nodes N_z and the number of solenoidal basis functions M should be related in the least by $N_z = (3M+10)/2$ in order to render the numerical quadrature exact due to the presence of the nonlinear terms.

4.1. *Linear stability for oblique magnetic field*

In order to test the solenoidal bases and the projection procedure, the linear stability of the conductive (no-motion) state is investigated under an oblique magnetic field that leads to critical Rayleigh values when the convective motion just sets in. The equations linearized around no-motion state

$$\frac{\partial \mathbf{u}}{\partial t} = -\nabla \Pi + PrRa_h \Theta \mathbf{e}_z + Pr\nabla^2 \mathbf{u} + Q_h Pr\,(Cos\chi \partial y + Sin\chi \partial z)\,\mathbf{b}, \tag{30}$$

$$\frac{\partial \Theta}{\partial t} = \frac{1}{2}\mathbf{e}_z \cdot \mathbf{u} + \nabla^2 \Theta, \tag{31}$$

are projected onto the dual space after the substitution of the expansions in terms of the bases, thus resulting in a system of ordinary differential equations

$$\begin{bmatrix} \left(\bar{V}_q^{(1)}, V_p^{(1)}\right) & 0 & 0 \\ 0 & \left(\bar{V}_q^{(2)}, V_p^{(2)}\right) & 0 \\ 0 & 0 & \left(\bar{T}_q, T_p\right) \end{bmatrix} \begin{bmatrix} \dot{a}_p^{(1)} \\ \dot{a}_p^{(2)} \\ \dot{b}_p \end{bmatrix} =$$

$$Pr \begin{bmatrix} \left(\bar{V}_q^{(1)}, (-\gamma^2 + \mathbb{D}^2)V_p^{(1)}\right) + & 0 & 0 \\ \left(\bar{V}_q^{(1)}, Q_h\,(Cos\chi\eta_m i + Sin\chi\mathbb{D})\,B_p^{(1)}\right) & & \\ 0 & \left(\bar{V}_q^{(2)}, (-\gamma^2 + \mathbb{D}^2)V_p^{(2)}\right) + & Ra_h\left(\bar{V}_q^{(2)}, T_p e_z\right) \\ & \left(\bar{V}_q^{(2)}, Q_h\,(Cos\chi\eta_m i + Sin\chi\mathbb{D})\,B_p^{(2)}\right) & \\ 0 & \left(\bar{T}_q, V_p^{(2)} \cdot e_z\right)/2Pr & \left(\bar{T}_q, \nabla^2 T_p\right)/Pr \end{bmatrix} \begin{bmatrix} a_p^{(1)} \\ a_p^{(2)} \\ b_p \end{bmatrix}, \tag{32}$$

for each wavenumber pair (ξ_m, η_n), where $\gamma^2 = \xi_m^2 + \eta_n^2$. The assumption of a time dependence in the form

Table I. Linear stability points for various angle χ and wavenumber k_c for constant oblique magnetic field $Q = 100$.

		Clever and Busse [10]	Present work (resolution)
Angle	k_c	Ra_c	Ra_c $(N_x \times N_y \times N_z)$
$\chi = 0°$	3.117	1707.8	1707.8 $(4 \times 4 \times 9)$
$\chi = 30°$	3.45	2281.3	2281.4 $(4 \times 4 \times 13)$
$\chi = 60°$	3.86	3290.7	3290.5 $(4 \times 4 \times 13)$
$\chi = 90°$	4.01	3757.2	3757.4 $(4 \times 4 \times 17)$

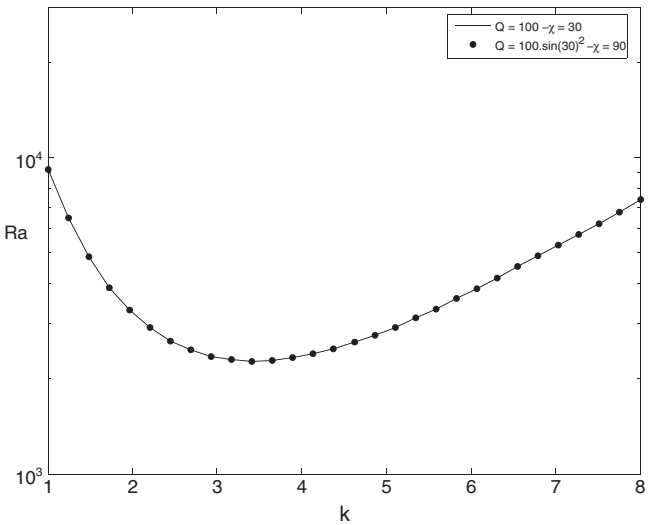

Figure 2. Comparing the result of the vertical magnetic field $QSin^2\chi$ with inclined magnetic field Q with angle $\chi = 30°$, at $Q = 100$.

$$\left[a^{(1)}; a^{(2)}; b\right] \propto exp(\varsigma t), \tag{33}$$

reduces the system to a generalized eigenvalue problem for the eigenvalues ς. The critical wavenumber k_c and Rayleigh number Ra_c values for $Q = 100$ and for various angle χ values are listed in Table I for the rightmost eigenvalue just crossing the imaginary axis. These are obtained at the selection of $n = 1$ and $m = 0$.

The horizontal component of the magnetic field has no effect on steady convection rolls, as stated in Chandrasekhar [2], Busse and Clever [10], and Burr and Müller [26]. This is shown in Figure 2 by comparing the effect of the inclined magnetic field Q at angle $\chi = 30°$ with the effect of the vertical component $QSin^2(30°)$ of the same field.

4.2. Linear stability for vertical magnetic field

The linearized Equations (30) and (31) are written for $\chi = 90°$ and then projected onto the dual space resulting in a reduced system of ordinary differential equations for each wavenumber pair (ξ_m, η_n), where $\gamma^2 = \xi_m^2 + \eta_n^2$, obtained. Then, the system is converted to a generalized eigenvalue problem for the eigenvalues ς. The critical wavenumber k_c and Rayleigh number Ra_c values for different Q values are listed in Table II for the rightmost eigenvalue just crossing the imaginary axis. These are obtained at the selection of $n = 0$ and $m = 1$. The corresponding

marginal stability curves for increasing Q values are plotted in Figure 3. These are in agreement with the linear analysis by Chandrasekhar in [2]. The solid circle marks in Figure 3 show the critical point for each marginal curve. The increase in the critical wave number with increasing Chandrasekhar number is associated with the lateral dimension of the convective rolls, as stated in [2]. This is explained in the study of Burr and Müller [28] by the lack of Joule dissipation for the vertical motions. Thus, the system reduces the scale of the horizontal motion in order to minimize the loss of Joule dissipation resulting in a decrease in the wavelength (increase in the wavenumber).

5. Nonlinear regime

For the numerical simulations in this regime, fully nonlinear model equations

$$\frac{\partial \mathbf{u}}{\partial t} = -(\mathbf{u} \cdot \nabla)\,\mathbf{u} - \nabla \Pi + PrRa_h \Theta \mathbf{e}_z + Pr\nabla^2 \mathbf{u} + Q_h Pr\,(Cos\chi \partial y + Sin\chi \partial z)\,\mathbf{b}, \tag{34}$$

Table II. Ra_c, for various Chandrasekhar number, Q and wavenumber, k_c.

		Chandrasekhar [2]	Present work (resolution)
Q	k_c	Ra_c	Ra_c $(N_x \times N_y \times N_z)$
0	3.12	1707.8	1707.8 $(4 \times 4 \times 9)$
50	3.68	2802.1	2802.1 $(4 \times 4 \times 11)$
500	5.16	10110.0	10110.0 $(4 \times 4 \times 21)$
6000	7.94	78391.0	78391.0 $(4 \times 4 \times 29)$

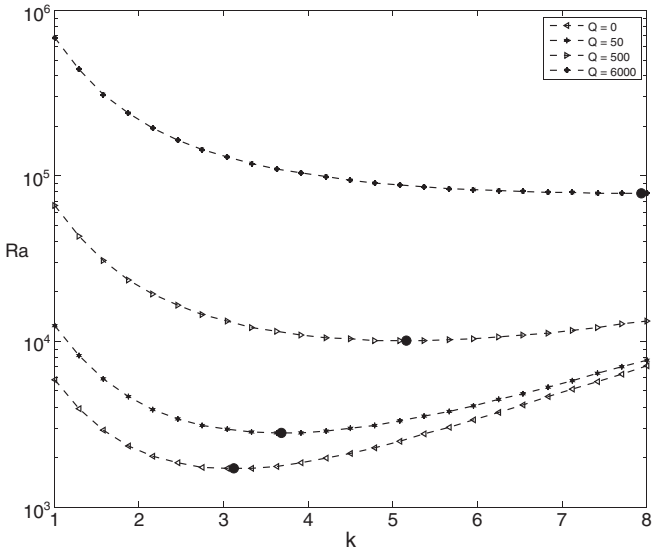

Figure 3. Marginal stability curves for different magnetic field strength Q values. Solid circles show corresponding critical points (k_c, Ra_c). ($R_c \to \pi^2 Q$ and $k_c \to (\frac{1}{2}\pi^4 Q)^{1/6}$ as $Q \uparrow$).

$$\frac{\partial \Theta}{\partial t} + (\mathbf{u} \cdot \nabla)\,\Theta = \frac{w}{2} + \nabla^2 \Theta, \tag{35}$$

are discretized in time

$$\left(5Pr\nabla^2 - \frac{12}{\Delta t}\right)\mathbf{u}^{n+1} = g^n, \tag{36}$$

$$\left(5\nabla^2 - \frac{12}{\Delta t}\right)\Theta^{n+1} = f^n, \tag{37}$$

where

$$\begin{aligned} g^n = &-23\left[-(\mathbf{u}\cdot\nabla)\,\mathbf{u} + PrRa\Theta e_z + Q_h Pr\,(Cos\chi\partial y + Sin\chi\partial z)\,\mathbf{b}\right]^n, \\ &+16\left[-(\mathbf{u}\cdot\nabla)\,\mathbf{u} + PrRa\Theta e_z + Q_h Pr\,(Cos\chi\partial y + Sin\chi\partial z)\,\mathbf{b}\right]^{n-1}, \\ &-5\left[-(\mathbf{u}\cdot\nabla)\,\mathbf{u} + PrRa\Theta e_z + Q_h Pr\,(Cos\chi\partial y + Sin\chi\partial z)\,\mathbf{b}\right]^{n-2}, \\ &-\left(8Pr\nabla^2 + \frac{12}{\Delta t}\right)\mathbf{u}^n + Pr\nabla^2\mathbf{u}^{n-1}, \end{aligned} \tag{38}$$

and

$$\begin{aligned} f^n = &-23\left[-(\mathbf{u}\cdot\nabla)\,\Theta + \frac{w}{2}\right]^n + 16\left[-(\mathbf{u}\cdot\nabla)\,\Theta + \frac{w}{2}\right]^{n-1}, \\ &-5\left[-(\mathbf{u}\cdot\nabla)\,\Theta + \frac{w}{2}\right]^{n-2} - \left(8\nabla^2 + \frac{12}{\Delta t}\right)\Theta^n + \nabla^2\Theta^{n-1}, \end{aligned} \tag{39}$$

using a semi-implicit scheme in which the nonlinear advection and magnetic terms are treated explicitly using the third-order Adams Bashforth method, and diffusion terms are discretized using an implicit third-order Adams Moulton method. This results in a

third-order accurate scheme in time. The resulting weak form of these equations after the projection procedure as in (32) is used to obtain the time evolution of the expansion coefficients. The computation is performed in the Fourier (wavenumber) space except for the nonlinear terms, which are computed in the physical space before transforming to the Fourier space.

5.1. Nonlinear analysis for oblique magnetic field

The numerical simulations are performed to study the effects of varying angle χ and Rayleigh number on the convective heat transport efficiency indicated by Nusselt number (Nu), which is the ratio of the heat transport with and without convection. The flow is chosen to take place in a convective box with the aspect ratio Γ [3.3 : 3.2] for Prandtl number, $Pr = 0.1$ and Chandrasekhar number $Q = 100$ in order to be able to compare with results of Busse and Clever [9] for the case $\chi = 90$. In Figure 4, Nu versus Ra values are shown for various direction angles of an external magnetic field fixed at $Q = 100$. The computation is started with the initial flow field just supercritical obtained using the eigenfunctions of the previous linear stability study.

Because the horizontal component of the magnetic field has the only effect of aligning the rolls along in the steady roll motion regime and the vertical magnetic field has an inhibition effect on the steady flow, the angle χ is an important parameter at the point where the rolls starts to oscillate. Chandrasekhar [2], Busse and Clever [10], and Burr and Müller [26] state that the horizontal component of the magnetic field has no effect on the steady convection rolls until roll solutions begin to loose its stability and oscillate, which are observed as kinks along the curves in Figure 4. These correspond to around $Ra = 12000$ for $\chi = 90°$, $Ra = 9000$ for $\chi = 60°$, and $Ra = 5000$ for $\chi = 30°$. The kinks appear earlier and in a more dramatic fashion for the angle χ closer to the horizontal in accordance

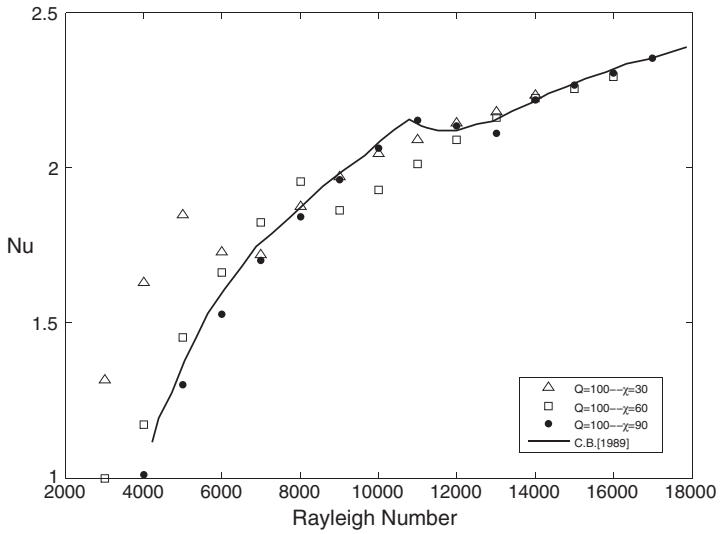

Figure 4. Nusselt versus Rayleigh number for different angle χ at $Pr = 0.1$, Γ [3.3 : 3.2] and $Q = 100$.

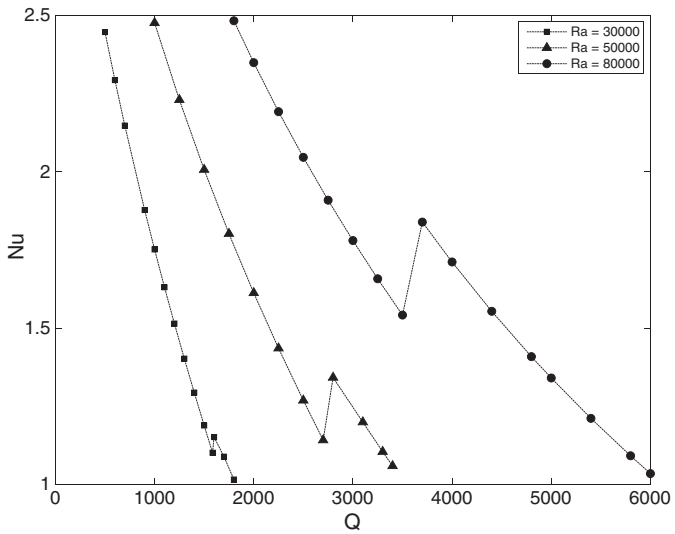

Figure 5. *Nu* versus *Q* for $Pr = 0.05$ at Γ [3 : 1.5].

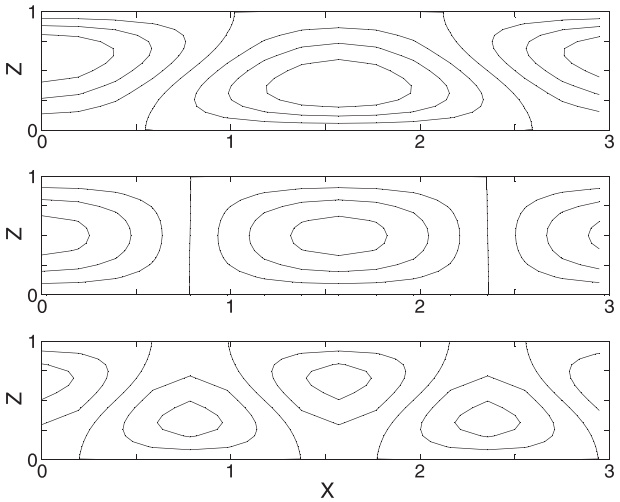

Figure 6. Isothermal contours in the *xz* plane during the transient stages $t = 0, 30, 60$ of restructuring from top to bottom graph, respectively, when initially $Q = 2500$ is suddenly set to 3000 at $Ra = 50000$, $Pr = 0.05$.

with the effects of the vertical and horizontal components of the imposed magnetic field. The horizontal component has more inhibition effect than the vertical component of the magnetic field after the onset of oscillations [10]. As the underlying convective motions develops with increasing Ra values, Nu values corresponding to different angle cluster in Figure 4. These extend the results presented in an earlier numerical study by Güray and Tarman [27].

5.2. Nonlinear analysis for vertical magnetic field

The numerical simulations at selected Rayleigh values are performed to study the effects of varying magnetic field strength Q on the convective heat transport efficiency. A liquid metal with $Pr = 0.05$ is selected in a layer with aspect ratio Γ [3 : 1.5] and subjected to a vertical magnetic field. The computation is started with the flow field obtained using the eigenfunctions of the linear stability study. It is known that the application of a vertical magnetic field suppresses the convective motions [11] as shown in Figure 5 by decreasing Nu values as Q increases, ultimately approaching to the conductive state with $Nu = 1$. In the process, kinks appear around $Q = 1400$ for $Ra = 30000$, $Q = 2500$ for $Ra = 50000$, and $Q = 3600$ for $Ra = 80000$. The kinks coincide with the increase in the number of rolls and thus decrease in the wavelength. This is also observed and discussed in [27]. This change in the roll pattern is shown in Figure 6, when $Q = 2250$ is increased to $Q = 3000$ for $Ra = 50000$ at the transient stages $t = 0, 30, 65$. All these runs are in the steady roll motion regime and use a typical dimensionless time step between 10^{-3} and 10^{-4}.

6. Conclusion

The approach presented in this paper is novel in the construction and the implementation of the solenoidal bases leading to the reduction of the model partial differential equations to a nonlinear system of ordinary differential equations in time variable as well as in the treatment of the solenoidal condition for the induced magnetic field variable in terms of derived solenoidal basis functions using the quasi-steady relationship. This approach is an important alternative to the numerical techniques for the treatment of the pressure variable in the case of incompressible flow and the treatment of the solenoidal conditions in Magnetohydrodynamics. The approach has been validated in linear stability analysis of conductive regime loosing its stability to convective regime under the influence of both oblique and vertical magnetic field. The results obtained in the numerical simulations are in good agreement with the studies in literature. With relatively low resolution requirement and ease in the implementation, the current approach is tested to be robust and efficient.

Acknowledgements

This study was supported by the Scientific and Technological Research Council of Turkey (TÜBİTAK-109M435) and State Planning Organization (BAP-08-11-DPT-2002K120510).

References

1. Davidson P. Magnetohydrodynamics in material processing. *Annual Review of Fluid Mechanics* 1999; **31**:273.
2. Chandrasekhar S. *Hydrodynamics and Hydromagnetic Instability*. Clarendon Press: Oxford, 1961.
3. Libchaber A, Laroche C, Fauve S. Period doubling in mercury, a quantitative measurement. *Journal de Physique Lettres* 1982; **43**:211.

4. Busse FH. Nonlinear interaction of magnetic field and convection. *Journal of Fluid Mechanics* 1975; **71**:(part 1), 193.
5. Nakagawa Y. Experiments on the inhibition of thermal convection by a magnetic field. *Proceedings of the Royal Society of London* 1957; **A240**:108.
6. Fauve S, Laroche C, Libchaber A. Effect of a horizontal magnetic field on convective instabilities in mercury. *Journal Physique-Lettres* 1981; **42**:455.
7. Busse FH, Clever RM. Stability of convection rolls in the presence of a vertical magnetic field. *Physics of Fluids* 1982; **25**:931.
8. Busse FH, Clever RM. Stability of convection rolls in the presence of a horizontal magnetic field. *Journal Of Theoretical And Applied Mechanics* 1983; **2**:495.
9. Busse FH, Clever RM. Nonlinear oscillatory convection in the presence of a vertical magnetic field. *Journal of Fluid Mechanics* 1989; **201**:507.
10. Busse FH, Clever RM. Finite amplitude convection in the presence of an inclined magnetic field. *European Journal of Mechanics* 1990; **9**:225.
11. Busse FH, Clever RM. Three-dimensinal convection in the presence of strong vertical magnetic field. *European Journal of Mechanics, B/Fluids* 1996; **15**:1.
12. Orszag SA, Kells LC. Transition to turbulence in plane Poiseuille flow and plane Couette flow. *Journal of Fluid Mechanics* 1980; **96**:159.
13. Kleiser L, Schumann U. Treatment of incompressibility and boundary conditions in 3-D numerical spectral simulations of plane channel flows, in Hirschel. *Proceedings of the E.H. (ed.): Third GAMM Conference on Numerical Methods in Fluid Mechanics, Vieweg, Braunschweig Modeling*, DFVLR, Cologne, 1980; 165.
14. Canuto C, Hussaini MY, Quarteroni A, Zang TA. *Spectral Methods: Evolution to Complex Domains and Applications to Fluid Dynamics*. Springer: New York, 2007.
15. Mössner R, Müller U. A numerical investigation of three dimensional magneto convection in rectangular cavities. *International Journal of Heat and Mass Transfer* 1999; **42**:1111.
16. Brackbill JU, Barnes DC. The effect of nonzero divergence on the numerical solution of the MHD equations. *Journal of Computational Physics* 1980; **35**:426.
17. Balsara DS, Kim J. A comparison between divergence-cleaning and staggered-mesh formulations for numerical magnetohydrodynamics. *Astrophysical Journal* 2004; **602**:(2-I), 1090.
18. Leonard A, Wray A. A new numerical method for the simulation of three-dimensional flow in a pipe. *NASA Technical Memorandu*, 1982.
19. Moser RD, Moin P, Leonard A. A spectral numerical method for the Navier–Stokes equations with applications to Taylor–Couette flow. *Journal of Computational Physics* 1983; **52**:524.
20. Mhuiris NMG. The construction and use of divergence-free vector expansions for incompressible fluid flow calculations. *NASA Technical Memorandum*, 1986.
21. Noack BR, Eckelmann H. A low-dimensional Galerkin method for the three-dimensional flow around a circular cylinder. *Physical Fluids* 1994; **6**(1):124.
22. Meseguer A, Trefethen LN. Linearized pipe flow to Reynolds number 10^7. *Journal of Computational Physics* 2003; **186**:178.
23. Pasquarelli F, Quarteroni A, Sacchi-Landriani G. Spectral approximations of the Stokes problem by divergence-free functions. *Journal of Scientific Computing* 1987; **2**:195.
24. Pasquarelli F. Domain decomposition for spectral approximation to Stokes equations via divergence-free functions. *Applied Numerical Mathematics* 1991; **8**:493.
25. Tarman IH. A Karhunen–Loeve based Galerkin approximation to Boussinesq equation. *Computer Methods in Applied Mechanics and Engineering* 1996; **137**(3-4):275.
26. Burr U, Müller U. Rayleigh-Bénard convection in liquid metal layers under the influence of a horizontal magnetic field. *Journal of Fluid Mechanics* 2002; **453**:345–369.
27. Güray E, Tarman IH. Thermal convection in the presence of a vertical magnetic field. *ACTA Mechanica* 2007; **194**:33.
28. Burr U, Müller U. Rayleigh-Bénard convection in liquid metal layers under the influence of a vertical magnetic field. *Physical Fluids* 2001; **13**:3247.